U.PORTO
FEUP FACULDADE DE ENGENHARIA
UNIVERSIDADE DO PORTO

Master Thesis in Mechanical Engineering

# Design of an Eco-Friendly Adhesively Bonded Impact Resistant Structure for Vehicles

**Author**:
Luís Miguel da Rocha Mâncio Corte-Real

**Supervisor**:
Prof. Dr. Lucas F. M. da Silva
**Co-Supervisor**:
Dr. Eduardo A. S. Marques

Master in Mechanical Engineering

Porto, July 2022

*To my family*

**Acknowledgements**

First, I would like to express my gratitude to Prof. Lucas da Silva, for the opportunity to be a part of this project, and for the knowledge and expertise shared throughout this last few months as the supervisor.

A special thank you to Dr. Eduardo Marques for the guidance along the project, the knowledge shared, constant availability and patience. Even during the times when setbacks were inevitable, his positive and optimistic attitude helped me surpass those difficult times.

To all the members of the Advanced Joining Processes Unit, AJPU, I have appreciated this past few months where I could enjoy the mutual help within its members, the constant availability, tips shared and friendship. It is a pleasure to know you all. A special appreciation goes to my fellow master's student fellows Frederico, Inês, Diogo and Bernardo for the solidarity, companionship and strong friendship developed.

This project marks the end of a long five year journey at Faculdade de Engenharia da Universidade do Porto, where lots of great memories where made and experiences lived. I would like to thank the institution and everyone that welcomed, influenced, taught and helped me develop not only as a future engineer, but also as a person.

I could not end without showing my gratitude to all my friends that were there for me all along the way and always provided me with valuable advice.

Finally, to my family and Ana, I appreciate the all the support given during these times and apologise for my constant unavailability.

**Abstract**

Nowadays, driven by demands for greater sustainability, the automotive industry is permanently seeking ways to develop lightweight structural components and, on the other hand, reduce the carbon footprint by proposing solutions which dispense with the unrecyclable and energy intensive materials such as synthetic composites and metallic alloys. Thus, an increase in the use of renewable materials in high performance products and structures, including wood, has been observed in the last few decades. Replacing the oil-based synthetic adhesives traditionally employed for eco-friendly adhesives has also been a topic of interest.

In this study, novel densified wood and wood/cork composites are proposed as substrates and its behaviour in an bio-adhesively bonded joint is analysed and optimised . Methods to enhance the mechanical properties of softwood through densification processes were reviewed and experimentally applied, with the purpose of using the end result in a joint bonded with a bio-adhesive, capable of absorbing large impacts. To mitigate delamination and the brittle behaviour of wood, cork agglomerates were introduced. Different configurations of single lap joints were manufactured to study the effect of the overlap length and strain on the performance of the joints in terms of failure load and energy absorption.

Furthermore, the work intends to provide a mechanical and fracture characterisation of the bio-adhesive and wood utilised with the aim of formulating a cohesive law for a numerical model to predict the behaviour of a single lap joint, using finite element analysis.

**Resumo**

Movida pela inescapável urgência em transitar para um mundo mais sustentável, a indústria automóvel tem procurado desenvolver estruturas mais leves e reduzir a sua pegada de carbono, propondo soluções que evitem o uso de materiais não recicláveis ou energeticamente intensivos tais como compósitos sintéticos e ligas metálicas. Desta forma, um aumento no uso de materiais renováveis em produtos de alto desempenho, incluindo madeira e seus derrivados, tem sido observado nas últimas décadas. Nesse mesmo sentido, os bioadesivos têm vindo a surgir como alternativa aos tradicionais adesivos de natureza sintética.

Neste estudo, inovadores compósitos de madeira/cortiça e madeira densificada são propostos e o seu comportamento em juntas ligada por bioadesivo é analisado e otimizado. Métodos para melhorar as propriedades mecânicas da madeira através de processos de densificação foram experimentalmente verificados, com o propósito de serem posteriormente utilizados numa junta ligada por um bioadesivo, capaz de absorver grandes impactos. De forma a evitar a delaminação e ultrapassar o comportamento frágil da madeira, foram também introduzidas camadas de aglomerado de cortiça na superfície dos materais a colar. Várias configurações de juntas de simples sobreposição foram produzidas para estudar o efeito do comprimento de sobreposição e das taxas de deformação no desempenho das juntas, sendo os resultados analisados em termos de carga de rotura e da absorção de energia.

Este trabalho pretende também fornecer uma caracterização de propriedades mecânicas e de fratura do bio-adesivo e da madeira utilizados, com o intuito de formular uma lei coesiva a ser introduzida num modelo numérico para prever o comportamento de uma junta de simples sobreposição, através de análise pelo método dos elementos finitos.

# Contents

**1 Introduction** **1**
1.1 Background and motivation . . . 1
1.2 Objectives . . . 1
1.3 Research methodology . . . 2
1.4 Thesis outline . . . 2

**2 Literature review** **5**
2.1 Adhesives . . . 5
2.1.1 General considerations . . . 5
2.1.2 Adhesive classification . . . 6
2.1.3 Loading modes and joint design . . . 8
2.1.4 Failure modes and joint design . . . 8
2.1.5 Strength prediction . . . 10
2.2 Wood: structure and properties . . . 14
2.2.1 Macrostructure . . . 15
2.2.2 Cellular structure . . . 15
2.2.3 Tracheids' cell wall structure . . . 16
2.2.4 Chemical composition . . . 17
2.2.5 Mechanical considerations . . . 18
2.3 Wood: delignification and densification . . . 19
2.4 Adhesively bonded timber joints . . . 24
2.5 Influence of cork particles in joint behaviour . . . 24

**3 Experimental procedures** **27**
3.1 Materials . . . 27
3.1.1 Wood . . . 27
3.1.2 Adhesive . . . 28
3.1.3 Cork . . . 28
3.2 Densification Process . . . 29
3.2.1 Chemical treatment . . . 29
3.2.2 Thermo-mechanical treatment . . . 29
3.3 Mould for densification process . . . 30
3.4 Joint manufacturing . . . 31
3.4.1 Wood joints . . . 32
3.4.2 Densified wood joints . . . 33
3.4.3 Wood/cork joints . . . 33
3.4.4 Considerations . . . 33
3.5 Additional cork modification . . . 34

3.6 Testing methods . . . 35
3.6.1 Bio-adhesive characterisation . . . 35
3.6.2 Thick Adherend Shear Test (TAST) . . . 35
3.6.3 Single lap joints . . . 36
3.6.4 Mode I and mode II fracture tests . . . 37
3.7 Data reduction scheme . . . 40

**4 Numerical details** **45**
4.1 General considerations . . . 45
4.2 Boundary conditions . . . 45
4.3 Mesh . . . 46

**5 Results and discussion** **49**
5.1 Bio-adhesive characterisation . . . 49
5.1.1 TAST . . . 49
5.1.2 DCB . . . 50
5.1.3 ENF . . . 52
5.2 Cork layer reinforcement . . . 53

**6 Conclusion** **57**
6.1 Conclusions . . . 57
6.2 Future work . . . 57

**References** **61**

**Appendices** **67**

**A Paper A** **69**

# List of Figures


1 Example of uniform stress distribution and stiffness increase of adhesively bonded joints in comparison to riveted joints. . . . . 6
2 Types of stresses acting on adhesive joints. . . . . 8
3 Most common joint configurations. . . . . 8
4 Schematic representation of cohesive and adhesive failure modes. . . . 9
5 Schematic representation of stress state and delamination in a joint. . 10
6 Fracture modes for an adhesive joint. . . . . 11
7 Schematic representation of fracture envelope approximations, using linear and quadratic criterion. . . . . 12
8 Schematic representation of traction separation laws. . . . . 13
9 Net carbon emissions in producing a tonne of various materials. . . . 14
10 Cross-section of a conifer species from the pine family, Douglas fir. . . 15
11 SEM images of Scots pine. . . . . 16
12 SEM images of English oak. . . . . 16
13 Schematic diagram of softwood cell wall structure. . . . . 17
14 Distribuition of main biopolymers within softwood tracheid. . . . . 18
15 Principal directions defined for anisotropic structure of wood. . . . . 19
16 Elastic modulus of wood polymers as a function of temperature and moisture. . . . . 20
17 Simplifed scheme representing the modification of the cellular structure of wood subjected to a delignification process via an alkaline media followed by a compression stage. . . . . 22
18 Effects of delignification treatment. . . . . 23
19 Illustration of the supplied cross-section dimensions of pine, highlighting the preferable ring orientation. . . . . 27
20 Bio-adhesive supplied for this work. . . . . 28
21 Wood blocks after chemical treatment. . . . . 29
22 Steps of the densification process. . . . . 30
23 Deformation of the lateral walls and resulting defects in the final product. . . . . 30
24 Deformation of the lateral walls and resulting defects in the final product. . . . . 31
25 Joint configurations. . . . . 32
26 Mould used for the fabrication of single lap joints. . . . . 34
27 Manufacturing of a reinforced cork layer. . . . . 34
28 Specification of a TAST specimen. . . . . 36
29 Schematic representation of a DCB test. . . . . 38
30 DCB specimen produced. . . . . 38

31 Schematic representation of a ENF test. . . . . 39
32 ENF specimen testing setup. . . . . 39
33 Graphic representation of the method used to determine the crack length correction, . . . . . 40
34 Schematic representation of equivalent crack and FPZ concepts. . . . 41
35 Illustration of the numerical model. . . . . 45
36 Illustration of the boundary conditions applied. . . . . 45
37 Mesh used in the simulations. . . . . 46
38 TAST specimen before and after the test performed. . . . . 49
39 Shear stress - displacement curve of the TAST specimen tested. . . . 50
40 P- obtained from DCB test. . . . . 51
41 R-curve obtained from DCB test. . . . . 51
42 Fracture surfaces - DCB. . . . . 51
43 P- obtained from ENF test. . . . . 52
44 R-curve obtained from ENF test. . . . . 52
45 Reinforced cork plate after production. . . . . 53
46 Load-displacement curve of a single lap joint before and after the reinforcement of the cork layer. . . . . 53
47 Fracture surfaces of WC joints with reinforced cork. . . . . 54

# List of Tables

1 Nominal elastic properties of pine wood. . . . . 28
2 Nominal strength properties of pine wood. . . . . 28
3 Testing campaign, highlighting the overlap length (in mm) tested for each condition. . . . . 37
4 Values of energy absorption for WC joints and reinforced WC joints. . 54

# 1 Introduction

## 1.1 Background and motivation

Nowadays, adhesive joining processes are used in a large range of industries, such as those operating in the automotive and aeronautical sectors. In these applications, adhesive bonding serves as a viable alternative to more common mechanical joining processes, such as the use of bolting, riveting, welding and brazing, presenting itself as a very interesting and highly competitive joining technology.

The growing implementation of adhesive joining processes in the engineering world derives from the unique advantages it presents when compared to traditional joining processes, namely the uniform stress distributions, higher stiffness and good load transmission capabilities, the ability to bond dissimilar materials, the possibility of automation of the manufacturing process, increased design flexibility and the generation of regular contours, among many others. [1, 2].

On the other hand, considering the path that is being followed towards vehicle electrification and global sustainability, the development of lighter and environmentally-friendly structures which are still capable of withstanding the required loads is of utmost priority. The use of materials such as metal alloys and synthetic composites produce a significant carbon footprint and requires more energy for its production than most renewable materials. In a similar manner, naturally sourced adhesives are slowly but increasingly being sought after as a viable alternative to the oil-based synthetic adhesives.

With this in mind, the need for eco-friendly adhesively bonded structures suitable for automotive applications has emerged. Recently, special treatments have become available to enhance the mechanical properties of wood through its densification. For bio-adhesives, there has also been a similar growth, driven by the availability of naturally derived precursors. Nevertheless, wood suffers from an issue which is common to synthetic composites: its low transverse strength promotes delamination in a joint, hampering the joint's ability to absorb large amounts of energy in an impact scenario, leading to a failure mode which is not easily predictable. The introduction of a cork agglomerate would thus able to reduce the brittle behaviour of densified wood while ensuring that the joint would present a safe and predictable failure mode.

## 1.2 Objectives

This thesis had four main objectives. The first of these was to carry out an optimisation of a wood densification process and to characterize the resulting material by means of experimental testing.

The second objective was to characterise the bio-adhesive employed in this work via mechanical testing of its stiffness, strength and toughness properties.

The third objective consisted of analysing and optimising the behaviour of the mentioned materials in an adhesive joint, by means of studying the effect of the overlap length and loading rate.

Lastly, a numerical approach suitable for reproducing the behaviour of single-lap joints with bio-adhesives and bio-substrates (using ABAQUS) was also targeted, serving as a tool to predict and optimise its behaviour, developed using some of the data obtained in the experimental part of the work.

## 1.3 Research methodology

The key objectives of this thesis are the following:

Perform a careful literature review, mainly focused on the state of the art regarding the densification processes of wood, used to improve its mechanical properties;

Carry out experimental tests to determine key properties of densified wood and bio-adhesives, namely through bulk tensile tests, thick adherend shear tests (TAST), double cantilever beam (DCB) tests, end notched flexure (ENF) tests;

Manufacture single lap joints in multiple configurations and study the effect of the overlap length and loading rate on the mechanical behaviour of the joint;

## 1.4 Thesis outline

This thesis is divided into seven main parts. This introductory chapter describes the background and motivation of this work, as well as a brief description of the problem in hand and the research objectives.

Chapter 2 starts with a review on the state of the art in the field of adhesive joints, their classification, failure modes and design methodologies. It includes a detailed description of the wood's structure and properties at a macro and micro scale before providing a review on the state of the art in relation to densification processes.

Chapter 3 clarifies the experimental procedures used throughout this work relating to the densification process, manufacturing of single lap joints, characterisation of the adhesive and characterisation of the densified wood.

Chapter 4 presents the development of a numerical model suitable to accurately predict the behavior of single lap joints which have been tested experimentally.

Chapter 5 contains results that were not included in the appended paper, such as the characterisation of the adhesive and additional tests performed.

Chapter 6 aggregates the main conclusions stemming from this research project, as well as suggestions to further improve and/or continue the work developed.

Finally, as an appendix, a paper is presented. It encompasses the assessment of the performance of the developed joints in terms of failure load and energy absorption when compared with other configurations. The effect of the overlap length is assessed by performing quasi-static tests while varying the overlap length of the single lap joints between 25 and 50 mm. Then, the overlap length is fixed and the effect of strain rate is evaluated by testing at three different conditions. Finally, the results are analysed and conclusions are taken.

# 2 Literature review

## 2.1 Adhesives

### 2.1.1 General considerations

An adhesive is a material that can be used to join surfaces together while effectively resisting their separation under load. Prior to the joining process, the materials used are called substrates, and afterwards are generally referred to as adherends. The interphase is defined as the physical region between the adhesive and the adherend with different chemical/mechanical properties from the respective materials, while the interface is the geometrical plane of contact between the surface and the two materials [1]. Intermolecular interactions between the substances originate attraction forces between them, creating an adhesion phenomenon [1]. On the other hand, cohesion derives from intermolecular interactions within the substance itself.

The use of adhesives based on synthetic polymers is seen as a viable alternative to conventional joining methods, such as bolting and riveting, and has grown in popularity over the last century. Multiple technological advances in this area allowed the development of structural adhesives which became relevant for multiple engineering applications, resisting significantly higher loads than non-structural adhesives or sealants [1, 3, 4].

General advantages regarding the use of adhesive bonding over conventional joining methods include:

Promotion of a uniform stress distribution, leading to higher stiffness and load transmission capabilities, ensuring cost and weight reductions - Figure 1;

Ability to bond thin sheets of material;

Allowing efficient plate bonding;

Capability to easily join dissimilar materials;

Easily automatable process;

Flexibility in joint design;

Possibility to have a smooth surface finish enabled by the lack of necessary discontinuities, namely holes.

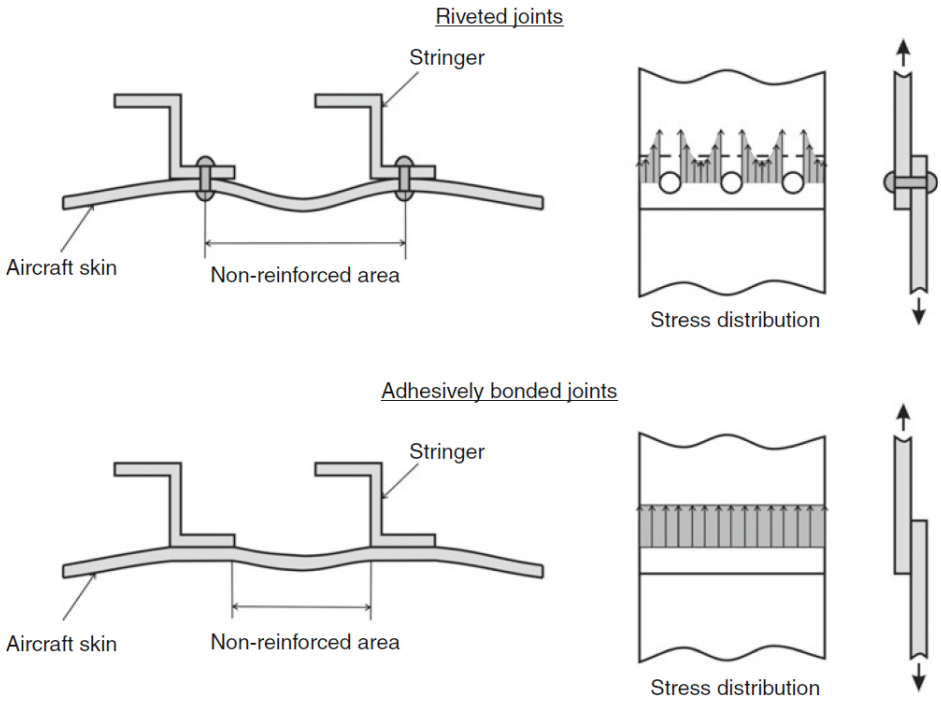


Figure 1: Example of uniform stress distribution and stiffness increase of adhesively bonded joints in comparison to riveted joints [1].

Regardless of the aforementioned benefits, the use of adhesives poses some issues and challenges such as [1, 2]:

A careful surface preparation is usually needed;

Generally requires the use of templates to maintain every component in the desired position, if the cure process is not instantaneous;

Curing conditions of adhesives usually involve long periods of time and high temperatures, which could be an issue from an economical/production point of view;

Polymeric nature of adhesives limits its applications in extreme temperature and moisture scenarios;

Unsatisfactory behaviour when subjected to peeling and cleavage stresses, which originate stress concentrations, leading to lower joint strengths;

Difficulties in performing quality control.

### 2.1.2 Adhesive classification

Adhesives' classification depends on several criteria:

Polymer base;

Functionality in the polymer "backbone";

Physical form;

Functional type;

Chemical family;

Method of application.

Regarding the first parameter, an adhesive may be sourced from either a natural or synthetic polymer. Natural based adhesives includes those which have a vegetable or animal origin and natural gums. On the other hand, adhesives that do not possess any sort of natural origin are considered as synthetic adhesives [1, 5].

The second parameter mentioned divides the adhesives between four categories: thermosets, thermoplastics, elastomers, and hybrids. Adhesives fall into the thermoset definition when the curing process of its polymer is irreversible due to chemical reactions at room or high temperature. Thermoplastics present a distinct behaviour, since they are usually cured by cooling down from a high-temperature molten state and present some environmental advantages due to the possibility of remelting the adhesive several times without affecting its properties. Regarding elastomers, their high elongation, toughness and peel strength make it stand out. Finally, hybrid adhesives result from an eventual combination of the above [1, 5].

In regards to physical form, adhesives can be applied as a liquid, paste, film or powder. Liquid adhesives have very low viscosity which requires the use of rolls, sprays or brushes and leads to good wettability. Paste adhesives are useful for filling large gaps and for application in vertical surfaces, owing to their high viscosity which limits their flow. Film adhesives are easier to handle and very effective for defining perfectly constant bondline thickness values. Powder adhesives are generally heated or dissolved in a solvent to acquire a liquid state prior to application [1, 5].

In terms of function, adhesives can not only be defined as structural or non-structural but are also referred to as hot-melt, conductive, water-base, pressure sensitive, ultraviolet cured, among other categorisations [1].

In terms of chemical family they can be characterised as epoxies, acrylics, polyurethanes, amongst others. Epoxies are thermoset structural adhesives being considered the most versatile ones since they are in general strong and brittle, but can be manufactured to be more flexible and tough without loss of tensile strength. Acrylics provide fast cure and high strength, however they are more expensive than epoxies. And polyurethanes are tough and flexible even at low temperature, but heat and moisture sensitive [1].

The application of the adhesive depends mainly on its viscosity and usually can be done via coating, spraying or brushing [1, 5].

### 2.1.3 Loading modes and joint design

To interpret the behaviour of an adhesive, understanding the type of stresses that a joint is subjected to is of utmost importance. Four types of stresses are commonly involved in the loading mechanism of a joint - normal, shear, peel and cleavage stresses - and are all represented in Figure 2.

(a) Normal. (b) Shear. (c) Peel. (d) Cleavage.

Figure 2: Types of stresses acting by adhesive joints. Adapted from [6].

In real applications, the adhesive joint is loaded in a way that a combination of stress types is usually present. The contribution of each stress usually depends on the way load is applied, the properties of both the adhesive and the substrates and the geometry of the joint. There are a few joint geometries which are very commonly employed, including the single-lap joint, since they are simple to manufacture and quite effective at transferring stresses. Double-lap joints, scarf joints and stepped-lap joints are examples of other geometries used (Figure 3) [7].

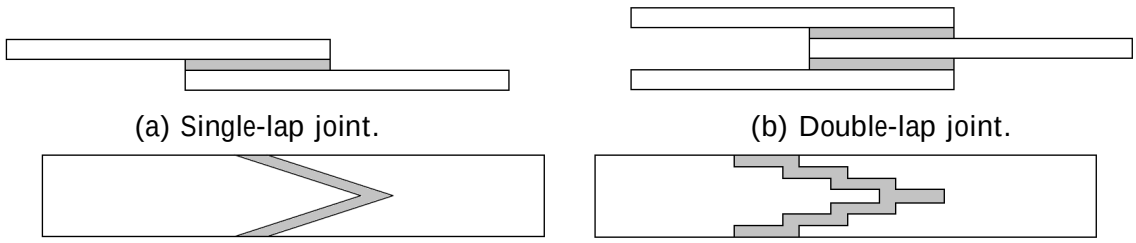

(a) Single-lap joint. (b) Double-lap joint.

(c) Scarf joint. (d) Stepped-lap joint.

Figure 3: Most common joint configurations. Adapted from [7].

### 2.1.4 Failure modes and joint design

An adhesive joint with homogenous adherends may present three failure modes, displayed in Figure 4: cohesive failure of the adhesive, adhesive failure and cohesive failure in the adherend.

Cohesive failure refers to the tear of the material internal cohesion. When a joint shows this type of failure both adherends remain covered with an adhesive layer.

When the joint fails at the interface between one of the adherends and the adhesive one is facing a so-called adhesive failure that normally occurs due to unsatisfactory surface preparation or an improper degreasing process.

Finally, a cohesive failure of the adherends occurs if loading conditions exceed the strength limit of the substrate's material, meaning that, in these eventual scenarios, the bondline is actually stronger than the materials the adhesive is joining.

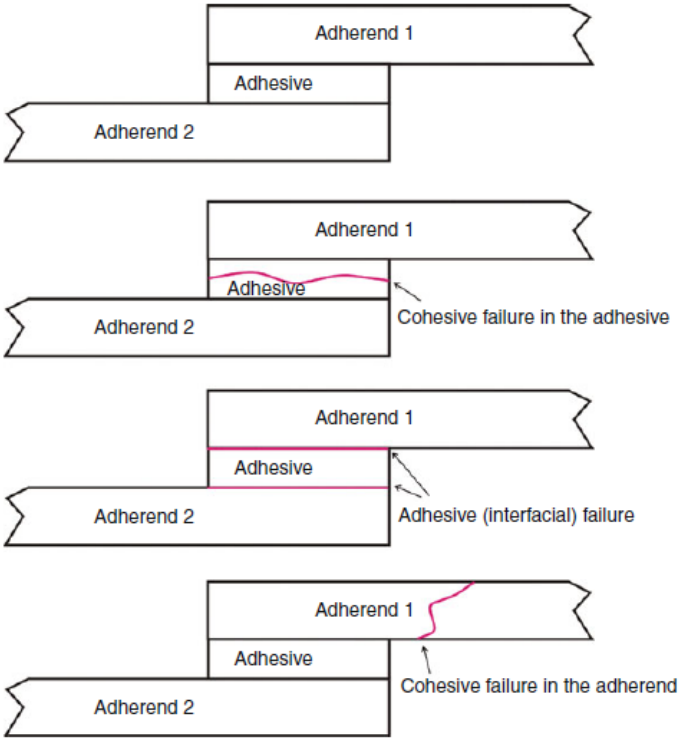


Figure 4: Schematic representation of cohesive and adhesive failure modes [1].

In the case where composites such as fibre reinforced plastics (FRP) or even timber are used as substrates an additional failure mode is possible. Due to the relatively low transverse tensile strength of these materials, peel stresses which peak at the ends of the overlap can originate an interlaminar failure by delamination, as schematised in Figure 5 [8].

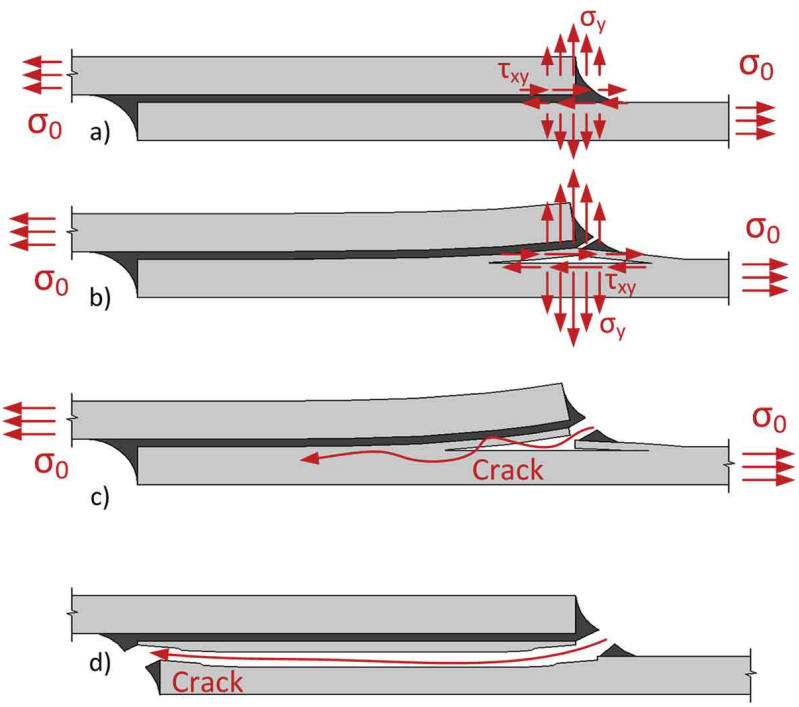


Figure 5: Schematic representation of stress state and delamination in a joint [9].

### 2.1.5 Strength prediction

To accurately predict the failure of adhesive joints, the consideration of the mechanical loads is not enough as it discards variables such as immeasurable defects, crack formation or even environmental conditions. This said, several approaches, namely continuum mechanics, fracture mechanics and damage mechanics, have been developed over the years to take these and other factors into account [10].

**Continuum mechanics**

A continuum mechanics approach defines both the adhesive and the adherends as continuous and does not consider the properties of the interface, assuming a perfect bond between the materials. Thus, the failure criteria is a function of two parameters: stress and strain. The reason this model fails to predict the failure of adhesive joints relies in the existence of singularities at the edges of the overlap, where stress values would always increase with mesh refinement in finite element analysis (FEA), therefore impeding convergence of the model. Several authors managed to solve this issue, but only developed approaches for continuous structures with a well defined geometry, limiting the applicability of this approach [11].

**Fracture mechanics**

In this approach, discontinuities are considered within the material, corresponding to the presence of cracks and other defects. These type of models quantitatively analyse the behaviour of structures containing cracks prior and during propagation, evaluating whether the crack size is higher than the critical failure size. The criteria

used in this approach are usually based on a stress intensity factor and a energy release rate [11].

When dealing with material discontinuities, generally a stress concentration factor - $K_t$ - is used to describe the stress distribution. Nonetheless, for sharp cracks it would not be possible to distinguish between similar geometries since at the crack tip the stresses would always tend to infinite. Consequently, a stress intensity factor was introduced, $K$, to represent into a scale parameter the stress distribution near the crack tip, commonly represented as:

$$K = Y \; {}_r \sqrt{a} \tag{1}$$

being $Y$ a non dimensional factor, that depends on the geometry and loading distribution, ${}_r$ the remote stress applied perpendicularly to the crack length, $a$. Crack propagation will occur when the stress intensity factor, $K$, is equal to a critical value - a material property defined as fracture toughness $K_c$ [11].

This method takes into account three failure modes: mode I, for normal loading; and mode II or mode III, for different types of shear loading, as observed in Figure 6.

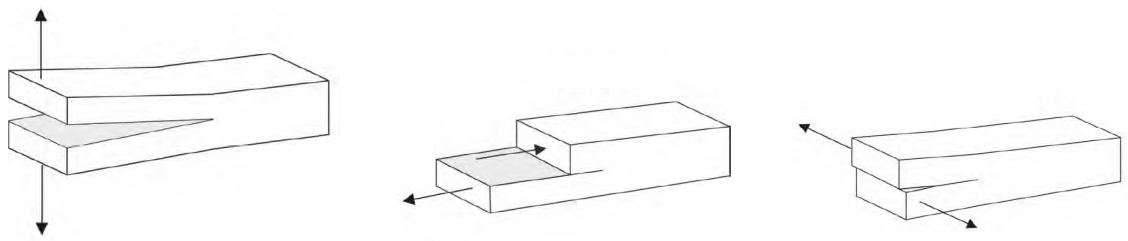

(a) Mode I. (b) Mode II. (c) Mode III.

Figure 6: Fracture modes for an adhesive joint [11].

On the other hand, an energy based criterion considers crack propagation when the available energy, $G$ - energy release rate (a function of the applied load) - is equal to a critical value where the crack propagates, $G_c$ - critical energy release rate (material characteristic) [11].

As the criteria mentioned above describe the same phenomenon, they can be associated by a physical relation, which for plane stress is [12]:

$$G = \frac{K^2}{E} \tag{2}$$

being $E$ the Young's modulus. And, for plane strain is [12]:

$$G = \frac{K^2}{E}(1 \quad {}^2) \tag{3}$$

where is the Poisson's ratio.

When comparing both methods, the critical energy release rate criterion is much more reliable, due to the difficulty of determining $K$ in certain contexts [11].

When using adhesives and considering their fracture behaviour, it is generally known that bulk materials tend to propagate cracks in mode I. However, in adhesive joints, due to the restrictions created by the adherends, cracks are forced to propagate in mixed mode I+II. This mode mixity can be represented by a mode ratio, given by [11]:

$$' = tan^{1} \sqrt{\frac{G_{II}}{G_{I}}} \tag{4}$$

For mixed mode cracks to propagate, it is necessary to combine the effects of both modes using suitable criteria, such as [11]:

$$\frac{G_{I}}{G_{Ic}} + \frac{G_{II}}{G_{IIc}} = 1 \tag{5}$$

being $G_{Ic}$ the critical energy release rate in mode I, $G_{IIc}$ the critical energy release rate in mode II, and and constants.

Knowing both mode I and II critical energy release rate, a fracture envelope can be elaborated by approximating the fracture behaviour using the linear or quadratic criterion, which can be seen in Figure 7.

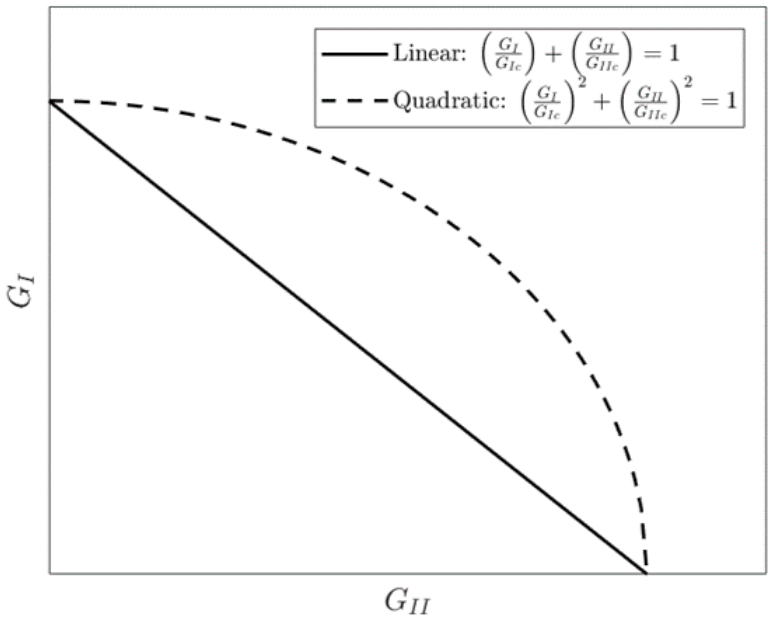


Figure 7: Schematic representation of fracture envelope approximations, using linear and quadratic criterion.

The main limitation of this model comes from its unsuitability to describe more than just damage propagation, i.e. damage initiation. [11].

**Damage mechanics**

To overcome the flaws observed in the aforementioned approaches, multiple methods were developed to not only include damage propagation but also take into consideration damage initiation. The most commonly used method to predict damage is a cohesive zone model (CZM), which is generally based on interface elements with no thickness, seeking to establish the bonding properties between two solid surfaces. Each element considers a damage variable that, after a stress criterion is satisfied, is used to simulate material degradation by applying a relaxation process based on a fracture energy criterion. Thus, such method avoids stress singularities and, at the same time, does not require the presence of pre-cracks or any intervention to initiate propagation [11].

The use of this technique to reproduce the behaviour of the adhesives is done via traction-separation laws, represented in Figure 8. A triangular, or bi-linear, law is generally used for its simplicity, being effective at modelling adhesives with a brittle failure process. A trapezoidal, or tri-linear, law is more adequate for use with ductile adhesives.

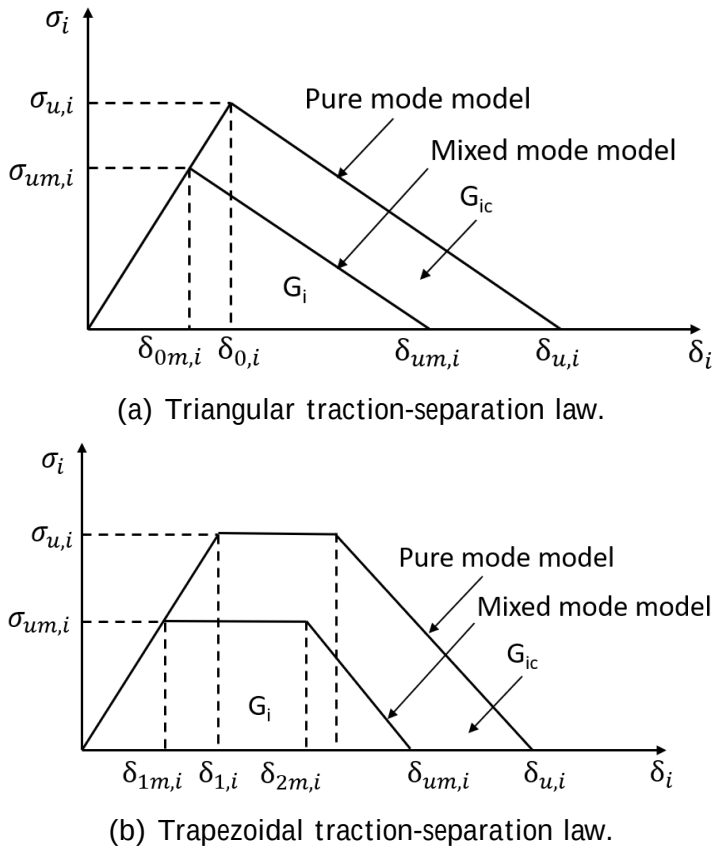


Figure 8: Schematic representation of traction separation laws, i=I,II.

## 2.2 Wood: structure and properties

Wood is well established as a natural and renewable resource that has long been used for a vast range of applications, from structural construction purposes to paper production. It is an abundant material worldwide which presents a competitive strength-to-weight ratio and is currently playing an important role in the race towards global sustainability, with it and its subproducts being known to have a lower carbon footprint than the production of traditional structural materials, as is illustrated in Figure 9 [13, 14]. It is important to clarify that the expressions "timber" and "lumber" are commonly employed to refer to wood. The difference between these relies in the processing stage. While "lumber" is used for wood that has just been cut from the tree and still contains the bark region, "timber" refers to a more processed stage where it has already been sawn into a intermediate product. However, in the United States, these words take the opposite meaning.

| Material | Net carbon emissions (kg C/t)[a,b] | Near-term net carbon emissions including carbon storage within material (kg C/t)[c,d] |
|---|---|---|
| Framing lumber | 33 | –457 |
| Medium-density fiberboard (virgin fiber) | 60 | –382 |
| Brick | 88 | 88 |
| Glass | 154 | 154 |
| Recycled steel (100% from scrap) | 220 | 220 |
| Concrete | 265 | 265 |
| Concrete[e] | 291 | 291 |
| Recycled aluminum (100% recycled content) | 309 | 309 |
| Steel (virgin) | 694 | 694 |
| Plastic | 2,502 | 2,502 |
| Aluminum (virgin) | 4,532 | 4,532 |

[a]Values are based on life-cycle assessment and include gathering and processing of raw materials, primary and secondary processing, and transportation.
[b]Source: EPA (2006).
[c]From Bowyer and others (2008); a carbon content of 49% is assumed for wood.
[d]The carbon stored within wood will eventually be emitted back to the atmosphere at the end of the useful life of the wood product.
[e]Derived based on EPA value for concrete and consideration of additional steps involved in making blocks.

Figure 9: Net carbon emissions in producing a tonne of various materials [14].

To ensure proper interpretation of wood's properties and general mechanical behaviour, it is crucial to have a basic understanding of its biological nature and structure.

### 2.2.1 Macrostructure

Figure 10 shows a cross section of a conifer species from the pine family. The pith is located in the center and is surrounded by the heartwood and sapwood regions. The heartwood is generally darker than the sapwood and is the zone that contains inactive cellular tissue which has ceased to conduct water and minerals. The interface between the sapwood and the bark is the cambium, being this the region where new wood is formed by means of cell division. The stem of most trees is consisted by several concentric annual rings where in each ring two regions can be distinguished - earlywood and latewood. As the name suggests, earlywood is formed early in the growing season and latewood is formed later and is denser and darker than the former. The age of the tree can be given by the number of rings present on the cross-section [15].

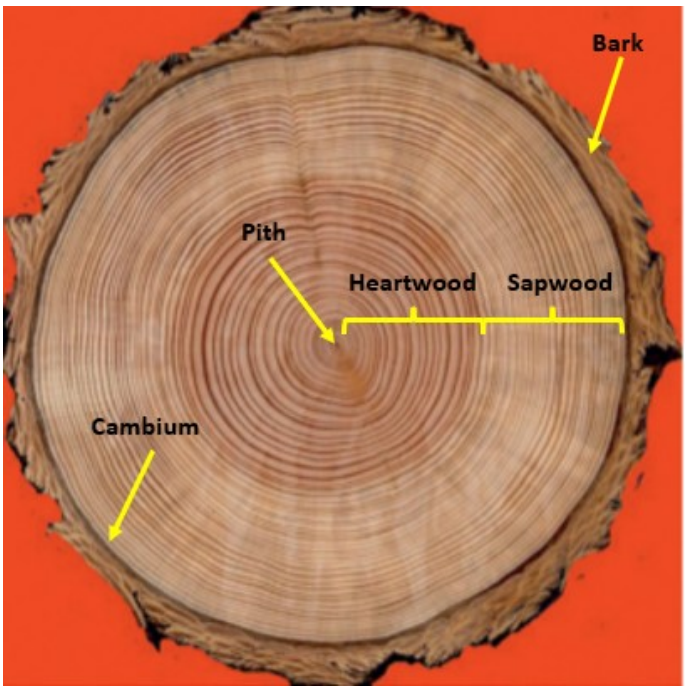


Figure 10: Cross-section of a conifer species from the pine family, Douglas fir [15].

### 2.2.2 Cellular structure

Regarding the cellular structure of wood, several differences exist between softwoods and hardwoods.

Softwoods contain two types of cells: tracheids and parenchyma cells. Tracheids are the basic cellular structure of the wood since they represent up to 95% of the total volume of wood. They are responsible for the vertical transportation of fluids and are the primary structural elements of the tree. These cells are aligned longitudinally, parallel to the stem and measure from 2 to 6 mm in length and 0.02 to 0.2 mm in width. Earlywood tracheids are thin-walled (2 to 3 µm) and have a large internal

cavity (lumen) to provide better conduction. Latewood cells play a more important role regarding mechanical strength, having smaller cavities and walls with a thickness around 7 µm [15,16]. On the other hand, parenchyma cells constitute the rays, small channels which allow the radial transportation of fluids between the tracheids [15,16]. SEM images of a softwood species where its cellular structure is noticeable are presented in Figure 11.

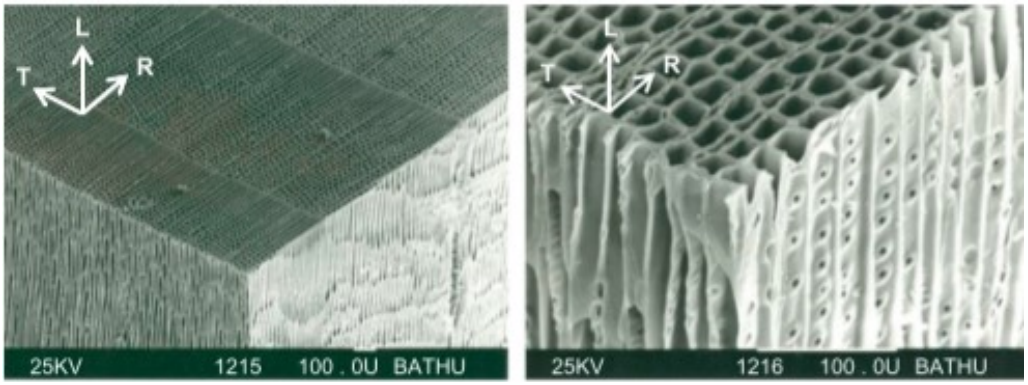


Figure 11: SEM images of Scots pine [15].

In contrast to softwoods, hardwoods present a much more complex cellular structure. The main difference resides in the combination of fibers and tracheids along with the existence of large longitudinal vessels, generally visible to the naked eye, which serve as the main fluid conductor. Radial cells also occupy a much larger volume in this case [13, 15]. In Figure 12 SEM images of a hardwood species are presented.

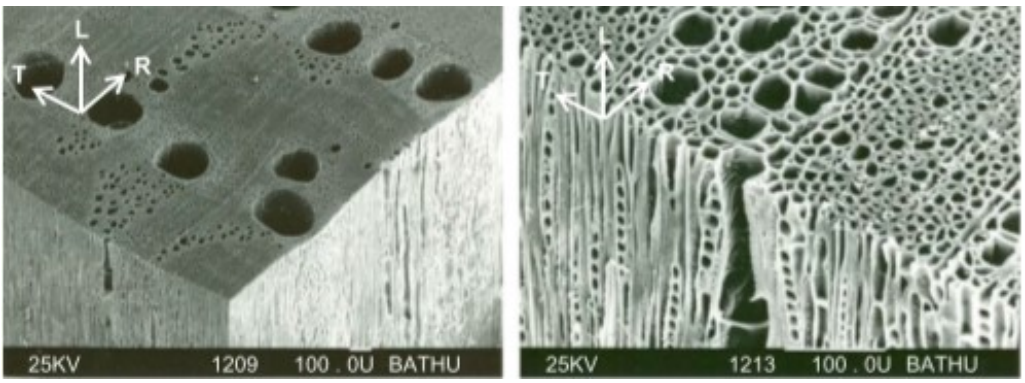


Figure 12: SEM images of English oak [15].

### 2.2.3 Tracheids' cell wall structure

As indicated previously, softwoods are mainly composed of tracheids. In its wall, from the direction of the perimeter towards the center, are found a middle lamella, a primary wall, a multilayered secondary walls and a cavity called the lumen [15, 17].

Middle lamella is an intercellular amorphous region which is responsible for adhering the neighbouring cells together. In the primary wall it is possible to observe

a random distribution of cellulose fibres. Due to the difficulty in distinguishing between the two, these regions are known as compound middle lamella (CML) [14]

The secondary wall comprises three layers (S1, S2 and S3) which present highly ordered cellulose microfibrils. The thickness of these layers are, commonly, 0.1-0.3, 1.0-5.0 and 0:1 µm respectively. The difference between these layers is mainly due to the orientation of the microfibrils. In S1 and S3, these are transversely orientated and arranged in a helical structure with an angle (in relation to the longitudinal axis) of 50°-70°for the S1 layer and 60°-90°for the S3. In contrast, S2's microfibrils, while presenting, as well, a helical structure, are axially orientated with an angle of 10°-30°. These properties, allied to the considerably larger thickness of this layer, make it the most important for providing structural properties to a living tree, since it carries most of the axial loading. The microfibril angle (MFA) in these layers plays a major role in the mechanical properties of the wood and several correlations can be done [17].

Figure 13 reveals the typical structure of a softwood's cell wall.

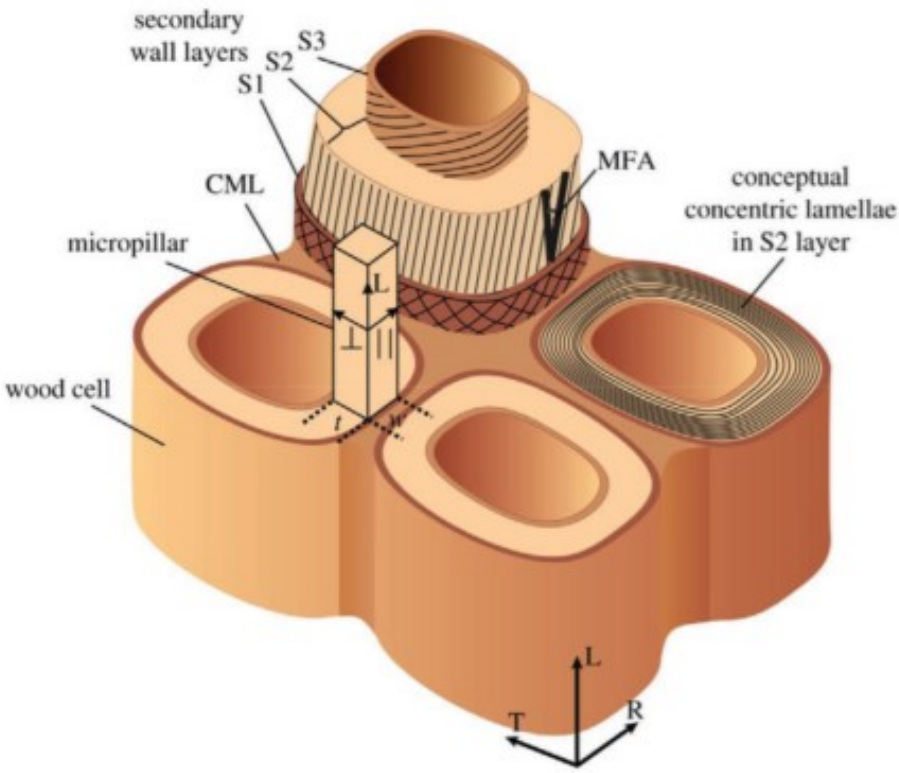


Figure 13: Schematic diagram of softwood cell wall structure [17].

### 2.2.4 Chemical composition

Wood can be seen as a composite material of three main biopolymers: cellulose, hemicellulose and lignin. Figure 14 shows the distribution of these constituents over a softwood tracheid cell. Cellulose microfibrils are arranged in hemicellulose

matrices and incrusted by lignin in the primary and secondary walls. The intercellular regions are mainly composed of lignin, acting as cementing material, providing rigidity against growth stresses and external loads.

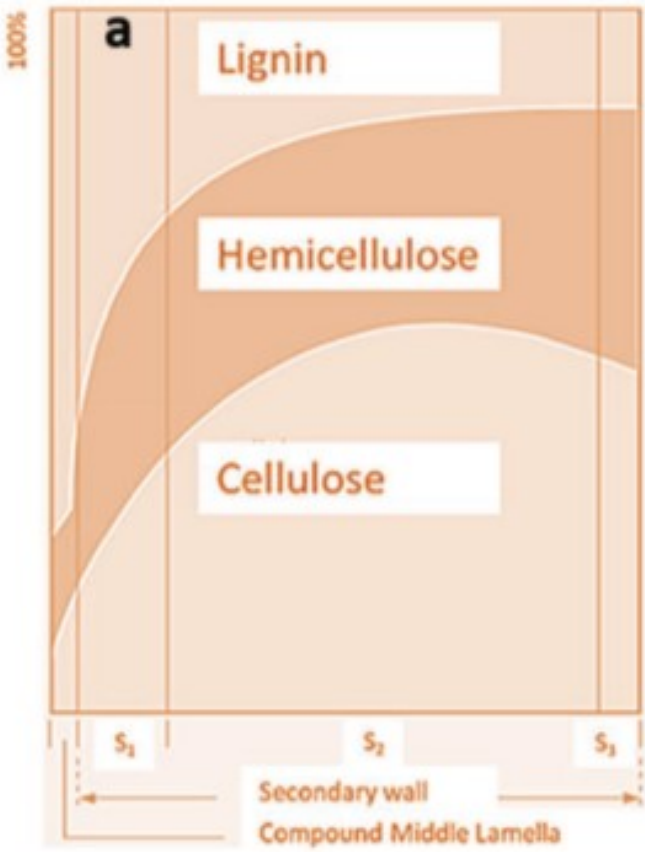


Figure 14: Distribuition of main biopolymers within softwood tracheid [17].

In this bio-composite material, the role of the fibre is portrayed by the cellulose microfibril, which is a link of several linear polymer chains by means of hydrogen bonding and Vand der Waals forces. These are combined to form larger fibrils and lamellae, providing a high tensile strength to the cell wall. Hemicelluloses are composed by several types of sugar units, being brached-chain polymers that link cellulose to lignin. As they are capable to permeate water, they provide flexibility and support in the cell wall. Lignin is a phenylpropanoid polymer, being a crucial component for assuring the structural integrity of the material, through its contribution for the stiffness and strength of the cell wall. It also protects the other two components from the attack of enzymes and microbial organisms [17, 18].

### 2.2.5 Mechanical considerations

Due to its anisotropy, the mechanical properties of wood depend on the considered direction and, being a natural material, are greatly affected by its complex anatomy. The fact that wood cells are predominantly oriented in the grain direction

originates a direction which ends up presenting much higher stiffness and strength values than the other two directions - the longitudinal axis of the trunk. From a macroscopic standpoint, wood is assumed to be a cylindrical orthotropic material, being the principal directions given by the longitudinal direction of the tree trunk (L), the radial (R) and tangential (T) directions, as observed in Figure 15. For this reason, and according to Hooke's law, the elastic behaviour characterisation of the material requires nine independent constants: three Young's modulus (E), three shear modulus (G) and three Poisson ratios ( ) that can be determined experimentally [9, 13].

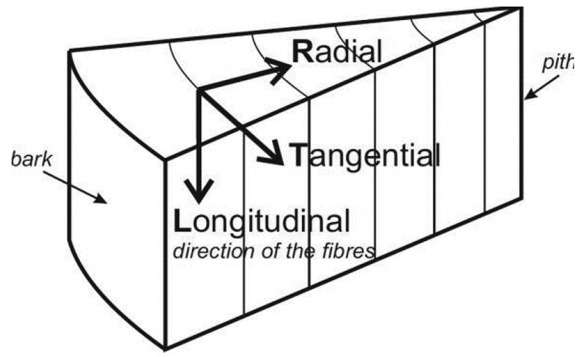


Figure 15: Principal directions defined for anisotropic structure of wood. Adapted from Valée et al. [9].

## 2.3 Wood: delignification and densification

The use of wood has recently gained importance, driven by the fact that this material has a low carbon impact and is a renewable resource, especially when considering forestry and harvesting practices which ensure the long-term health and diversity of the forests [14]. For this reason, the interest relies more on the utilization of timber derived from fast-growing species. However, these normally result in a low wood density and poor mechanical properties, which strongly limits its use in advanced engineering structures and applications [19, 20]. Nevertheless, an eventual increase of these materials' density has the potential to turn these materials into high value and high-performance products, acting as a substitute to harder species or conventional alloys for more demanding applications [21].

To extend the range of possible wood applications, including as substrates in structural bonded joints, several technological processes have been proposed in recent years to increase wood density and its mechanical properties, most of which involve thermo-hydromechanical (THM) treatments [21]. The reason for this relies on the viscoelastic nature of wood, which make its mechanical properties depend on time, temperature, and moisture. Like other amorphous polymers, the lignin and hemicellulose present in wood also have a glass transition temperature ($T_g$) that marks the transition between a stiff and brittle behaviour (below $T_g$) and a rubbery

and compliant one (above $T_g$). Such behaviour is promoted by polymer mobility and a consequent rearrangement of the molecules enabled by temperatures above the $T_g$ of these polymers, which allows for large deformation under compression to occur through buckling of the cell walls, instead of a fracture process [22–24]. This temperature is estimated to be in the 167-217°C range for hemicellulose and 134-235°C for lignin in dry condition. Notwithstanding these relatively high values, the $T_g$ is found to be greatly influenced by moisture, as an increase in the moisture content of wood results in a decrease of the $T_g$. It acts as a plasticizer, reducing the secondary bonding between the polymer chains and allowing the polymer molecules to move around more easily [23]. In Figure 16, the influence of moisture in the $T_g$ of the wood constituents is illustrated.

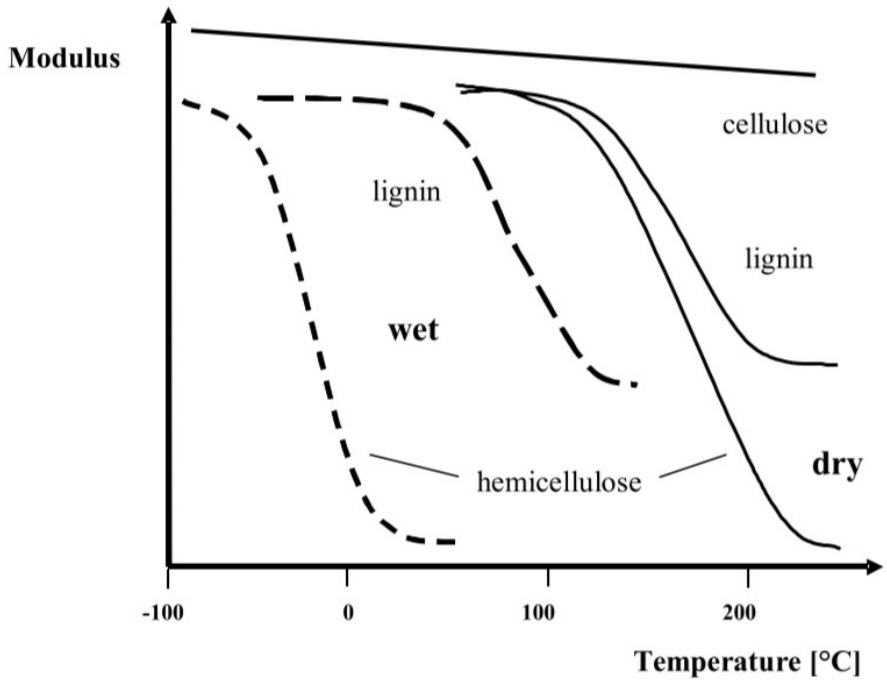


Figure 16: Elastic modulus of wood polymers as a function of temperature and moisture [23].

A major drawback associated to the densification process has to do with the resultant moisture sensitivity which can lead to irreversible swelling – a phenomena known as "set-recovery". The reasons for this are attributed to the release of elastic energy stored in the cellulose macromolecules and the unbroken and, therefore, not reformed covalent and hydrogen bonds between the polymers [23, 25, 26]. Sadatnezhad et al. focused on increasing the density in the region beneath the surface of poplar wood by applying a THM treatment. The set-recovery after three wet-drying cycles was 44% [27]. Laine et al. experienced a set-recovery of 60% after water-soaking densified Scots pine samples. However, this was was almost eliminated by the application of a thermal modification treatment after the com-

pression [24]. Schwarzkopf reduced the set-recovery on densified poplar, spruce and beech samples by impregnating a phenol resin into the cell lumens prior to the THM treatment [26].

Chemical pre-treatments have also been successfully employed to mitigate the aforementioned problem while increasing the level of densification [20]. These are based on delignification processes which have for long been used, for example, in the paper industry, as they lead to more exposure of cellulose microfibrils (originally involved in the lignin and hemicellulose matrices). They allow partial or complete removal of lignin (and inevitably hemicellulose) and generally consist in the utilization of a boiling alkaline media to enable complex reactions which result in the breakage of lignin-hemicellulose bonds, degradation and solubilization of lignin and hemicellulose while promoting the hydrophilicity of the material. The reason for this derives from the fact that lignin is the main hydrophobic component of wood so its removal improves the cell wall accessibility towards moisture uptake. The end result is a more flexible and formable material with increased porosity which retains its fibrous cell wall structure and is easily compressed without defects, profiting from the reduced transverse rigidity of the cell walls induced by the lignin removal. [17,28–30]. The reason that allows densified wood to maintain its integrity while improving its mechanical properties, even without a significant lignin matrix present (which acts as a cementing and structural material), lies in the formation of fixed H-bonds between the cellulose fibrils upon drying under compression, enabled by free OH groups [17,29]. Physical interlocking of the cellulose fibres is also considered to be a reason [29]. Figure 17 presents a simplified scheme of the densification process with a prior delignification treatment applied.

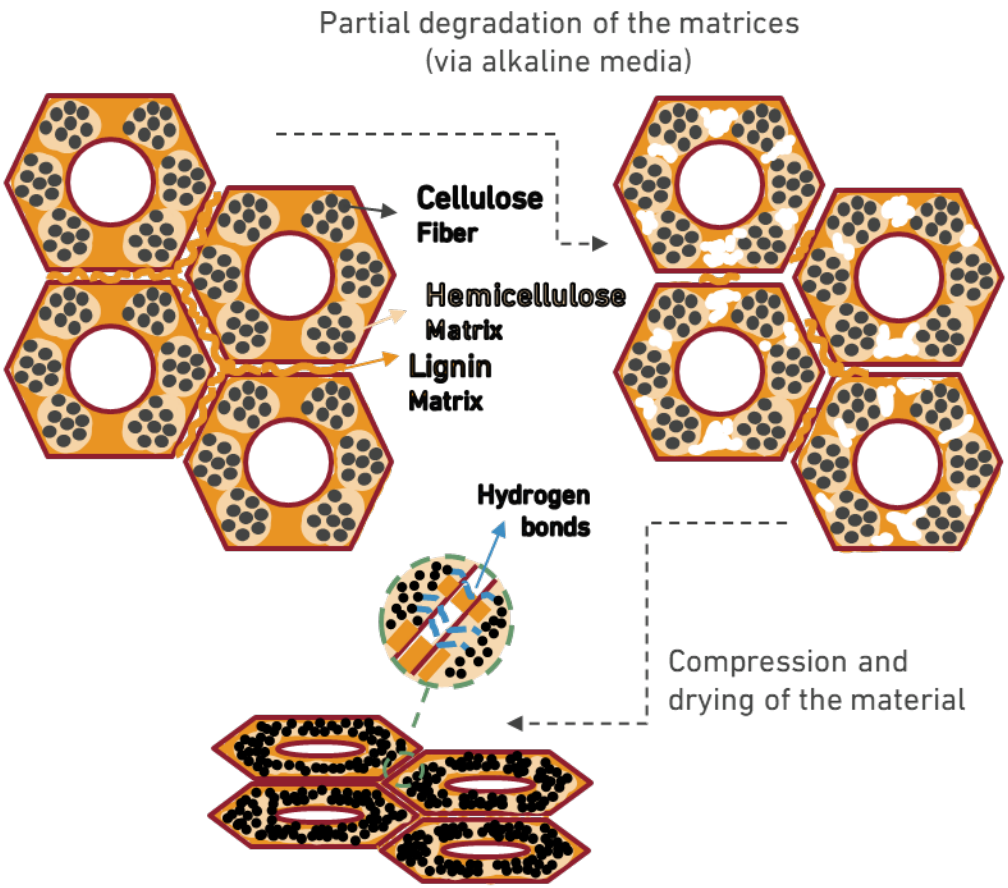


Figure 17: Simplifed scheme representing the modification of the cellular structure of wood subjected to a delignification process via an alkaline media followed by a compression stage.

Several authors have used methods based on wood delignification to assist densification processes. Song et al. proposed a boiling process in a solution of NaOH and $Na_2SO_3$ followed by hot pressing of several species of softwood in the radial direction, obtaining a specific strength higher than most of the structural alloys (422.2 36.3 MPa $cm^3$ $g^{-1}$ and a tensile strength of 587 MPa. They studied the effect of lignin removal percentage on the final properties of the material (Figure 18b) and the results showed a higher increase in density for 45% lignin removal, being the resultant chemical composition presented in Figure 18a. To vary the degree of delignification, only the boiling times were adjusted. Dimensional stability of the densified samples under moisture attack was evaluated and, after 128 h at 95% relative humidity, an increase of 8.4% in thickness was observed, although only resulting in a modest drop regarding tensile strength (16%). Furthermore, it was verified on SEM images that samples which were not chemically treated prior to the compression stage were left with many gaps in between collapsed cell walls.

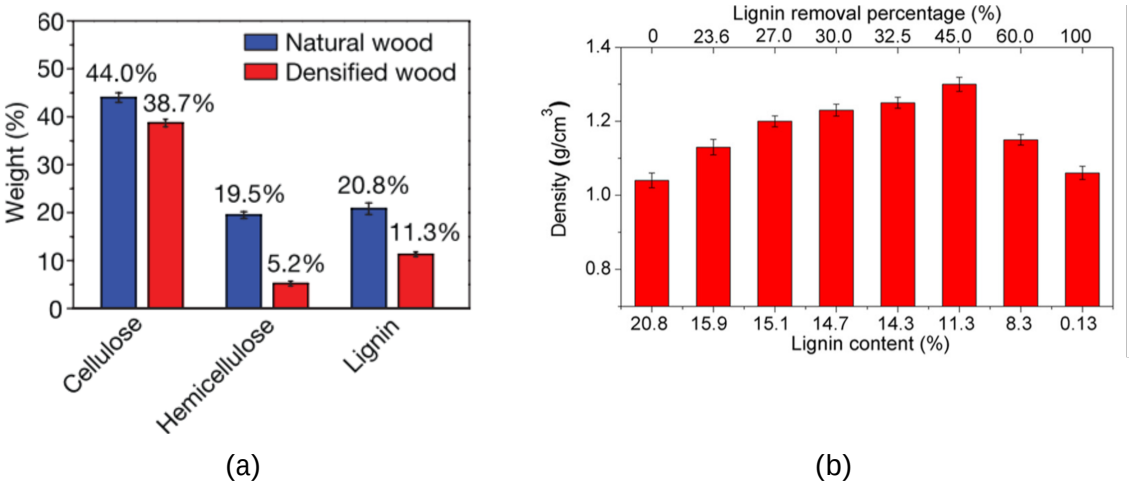


Figure 18: Effects of delignification treatment: a) Chemical composition of the wood after optimal chemical treatment. b) Effect of lignin removal percentage on the final density of the wood [20].

Novel et al. performed a similar chemical treatment before intercalating nanoparticles of silicon carbide or graphene oxide to samples of giant reed and proceeding to the pressing stage. Five types of samples were investigated: natural reed, thermo-compressed reed (without chemical treatment), densified reed, densified reed in intercalation of SiC particles, and densified reed with intercalation of GO particles. The addition of the nanoparticles was shown to increase the mechanical properties of the densified samples regarding Young's modulus, tensile strength and flexural strength (more evident with SiC particles) despite the resulting density being quite similar (almost the triple value of natural reed). This particle intercalation also resulted in a reduced water uptake by the wood. Densified samples without particle addition proved to have better flame retarding properties when compared to natural wood and particle-filled samples [31]. Shi et al. followed a similar procedure with *Abies* wood samples and obtained an average compression ratio of 80% in the radial direction of the wood. The colour modification on the resulting densified samples was considered to occur as a synergistic effect of chemical pretreatment, hot-pressing and post mechanical fixation. To quantify these changes, chromacity values were measured. Regarding mechanical characterization, the results show that the tensile strength and Young's modulus obtained showed an increase of 97% and 346%, respectively [32]. Wang et al. studied the microstrutcture, chemical properties and dimensional stability of densified poplar wood through delignification. Complete cell wall collapse was observed near the surface of all samples and chemical analyses showed that delignification occured mainly near the surface of the blocks and enhanced hydrogen bonding among the cellulose fibres. The set-recovery was found to decrease with an increase in alkali dosage [33].

## 2.4 Adhesively bonded timber joints

As is the case for other materials, timber joints also benefit from adhesive bonding. In this area, the use of mechanical fasteners (including nails, bolts and and screws) have been the most commonly employed solution. Notwithstanding, these usually result in disruption of wood fibres, promote local stress concentrations, increase cost and frequently allow water to ingress into the structure [9]. The shear strength of a joint is a widely used indicator to evaluate the quality of glued wood products. The factors which affect it include the physical and chemical properties of the adhesive, the physical and structural properties of the wood substrates and the parameters of the process [34, 35]. Another indicator commonly employed to measure the quality of a wood joint is WFP (wood failure percentage), which defines the percentage of area in the joint where the failure occurred in the wood. The higher this value is, the better the quality of the bondline and , in the limit, the resistance of the joint is only function of the wood [36]. Due to the cellular nature of wood, absorption of the adhesive by the substrate occurs and its level depends largely on the density of the wood and, consequently, on its porosity. Follrich et al. studied the effect of the density of spruce on the quality of end joints and the results showed the bond strength increased as the density increased [37]. On the other hand, the same authors conducted further research on balsa wood end joints considering differing densities. The increase in density promoted a rapid decrease in WFP and a slight increase in bond strength [38].

## 2.5 Influence of cork particles in joint behaviour

Structural bonded joints can also benefit from the inclusion of biomaterials within the adhesive layer. To increase the toughness of an adhesively bonded joint, the inclusion of cork particles can also be considered [39]. Akhavan-Safar et al. studied the effects of natural particles on the micro failure mechanisms and static strength of an epoxy adhesive and obtained a higher energy absorption and toughness for bulk specimens containing 1% in volume of cork particles. The results also showed that the optimum amount of cork may vary depending on the loading conditions [40]. da Silva et al. focused on the incorporation of cork microparticles on an epoxy adhesive as a tool to promote cohesive failure in single-lap joints. The results have shown that for some certain conditions the performance of the joint was improved, although the failure mechanisms in these cases was adhesive [41].

# 3 Experimental procedures

In this chapter, the experimental procedures required for this work are fully described and carefully analysed,

## 3.1 Materials

### 3.1.1 Wood

In this work, pine timber (*Pinus Pinaster*) was the main material employed. It was supplied in two distinct cross-section dimensions. The beams which had a larger cross-section were used for the densification process and other procedures, whereas the smaller cross-sectioned timber was only employed in the manufacturing of the single lap joints.

For the dimensions of the larger beams destined for densification, the maximum load capacity of the hot-press was found to be an issue. The multiplication of the wood block area in contact with the press plates naturally reduced the pressure applied for a given force considered. For large wood samples, the load increment required to maintain the same pressure level easily surpassed the maximum capacity of the press. Thus, a trade off had to be considered between the cadence of production and the level of densification attained.

It must be stated that having symmetry of the wood rings in relation to a central vertical axis was not always possible, since the supplier could not always guarantee it. However, the preferable orientation of the rings is shown in Figure 19. The density of the supplied timber varied in the range between 0.564 g/cm$^3$ and 0.670 g/cm$^3$.

Figure 19: Illustration of the supplied cross-section dimensions of pine, highlighting the preferable ring orientation.

The nine elastic constants and strength properties on the longitudinal (L), radial (R) and tangential (T) directions can be determined experimentally. Moura and

Dourado have performed these experiments for this type of pine wood and the results they have obtained are summarized in Tables 1 and 2.

Table 1: Nominal elastic properties of pine wood.

| $E_L$ [GPa] | $E_R$ [GPa] | $E_R$ [GPa] | $_{LT}$ | $_{LR}$ | $_{TR}$ | $G_{LR}$ [GPa] | $G_{LT}$ [GPa] | $G_{TR}$ [GPa] |
|---|---|---|---|---|---|---|---|---|
| 12.0 | 1.91 | 1.01 | 0.51 | 0.47 | 0.31 | 1.12 | 1.04 | 0.29 |

Table 2: Nominal strength properties of pine wood.

| $_L$ [MPa] | $_R$ [MPa] | $_T$ [MPa] | $_{LR}$ [MPa] | $_{LT}$ [MPa] | $_{RT}$ [MPa] |
|---|---|---|---|---|---|
| 97.5 | 7.9 | 4.2 | 16.0 | 16.0 | 4.5 |

### 3.1.2 Adhesive

The adhesive used in this work, shown in Figure 20, was entirely developed by Professor João Bordado and his research team, at Instituto Superior Técnico. It is a polyurethane based bio-adhesive, since 70% of its content derives from natural precursors. It has been especially formulated to provide good adhesion to both wood and cork. This bio-adhesive is not yet a commercial product.

Figure 20: Bio-adhesive supplied for this work.

### 3.1.3 Cork

The cork utilized for this work was supplied by Sedacor, as agglomerated cork sheets with a thickness of 1 mm and also as a standalone granulate, devoid of any agglomerating agent.

## 3.2 Densification Process

To obtain specimens of densified wood, blocks of the aforementioned natural pine wood were first subjected to a densification process. The process was based on the method proposed by Song et al. [20] and consisted of two main steps: a chemical treatment and a thermo-mechanical stage.

### 3.2.1 Chemical treatment

Each of the wood blocks, with the aforementioned cross-section dimensions and an average length of 240 mm, was weighted and subjected to a chemical treatment prior to the compression stage. The chemical bath consisted of a aqueous solution of 2.5 M of NaOH and 0.4 M of $Na_2SO_3$. 250 g of NaOH and 125 g of $Na_2SO_3$ were carefully dissolved in 2.5 L of deionized water inside a stainless steel container (Figure 21). The wood block was then submerged on the solution and the container was kept in an oven at boiling temperature (100 °C) for 7 hours. Finally, two baths in boiling deionized water (1h) followed this step, helping to remove any chemicals that remained in the wood.

Figure 21: Wood blocks after chemical treatment.

### 3.2.2 Thermo-mechanical treatment

Immediately after removal from the deionized water bath, the wood block was placed in a hot-press for 24h at 100 °C and compressed under 3 MPa of pressure. In initial attempts, the blocks were placed directly on the press plates, with no lateral restriction. However, to reduce the amount of defects on the resulting product, a steel mould was introduced in the process to restrain movement in the lateral direction. The blocks were always cooled down to room temperature in 5h before being removed from the hot press, weighted and measured. The steps of the complete process are summarised in Figure 22.

Figure 22: Steps of the densification process.

## 3.3 Mould for densification process

After the first timber blocks were compressed directly on the hot-press, several issues were noted. The thickness reduction was significant, being mostly the result of a collapse of the lateral walls of the block, which prompted a large increase in the width of the final product, as shown in Figure 23. Consequently while the specimen was almost flattened, the density increase was not satisfactory and a large number of defects and cracks was present in those samples.

(a) Deformation of the walls under compression.

(b) Example of a densified block.

Figure 23: Deformation of the lateral walls and resulting defects in the final product.

Bearing that in mind, a new steel mould was designed and produced (Figure 24), seeking to ensure that, under compression, any movement only occurred in the vertical condition, fixing the lateral walls between steel plates which were connected to each other via transversely positioned small plates bolted at their ends. The

dimensions of the mould were based on the dimensions of the timber blocks and a 1 mm tolerance was added to each side. The punch was bolted to a large plate which leaned against the top plate of the press. Several holes were drilled in the bottom of the plates to allow for excess liquid to freely escape from the wood block.

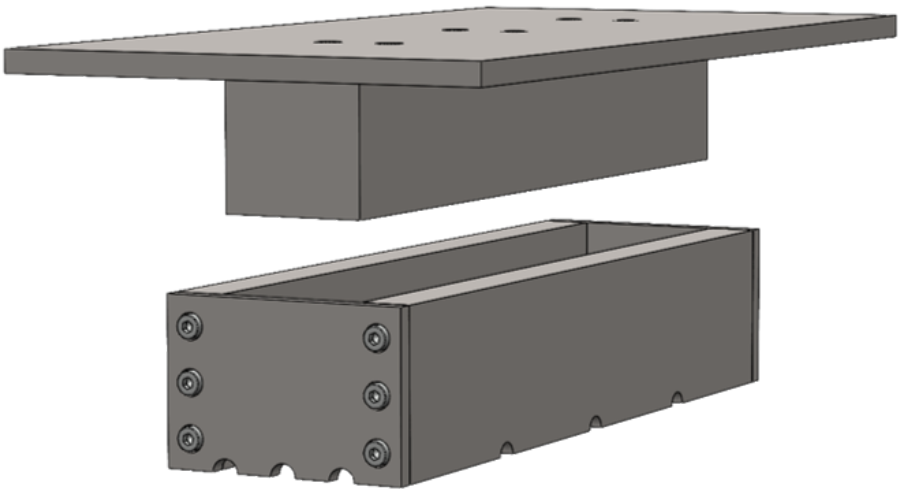

(a) 3D model of the mould.

(b) Mould in use.

Figure 24: Deformation of the lateral walls and resulting defects in the final product.

## 3.4 Joint manufacturing

For the manufacture of single lap joints, three different configurations were considered:

Single lap joints with wood substrates (W) - Figure 25a;

Single lap joints with densified wood substrates (DW) - Figure 25b;

Single lap joints with wood substrates coated with a cork agglomerate (WC) - Figure 25c.

(a) Illustration of W single lap joint.

(b) Illustration of DW single lap joint.

(c) Illustration of CW single lap joint.

Figure 25: Joint configurations.

### 3.4.1 Wood joints

The preparation of these joints involved manually cutting of the substrates from a profile with the cross-section of 25x4 mm mentioned in Figure 19. All the samples were cut with a length of 10 mm. The bio-adhesive (Section 3.1.2) was used to bond the substrates and was carefully applied in the joint, considering two overlap lengths: 25 and 50 mm. The thickness of the bondline was not controlled, since the adhesive requires zero-thickness condition to achieve a bond. This is due to the very high viscosity it exhibits, precluding the formation of a large layer. Pressure was applied along the overlap length through manual clamps and the joints were cured for 8 hours at 50 °C.

### 3.4.2 Densified wood joints

Densified joints were prepared in the same manner as the previous ones. Nevertheless, in this case the substrates for these joints were cut from the densified blocks, with the same dimensions as reported before.

### 3.4.3 Wood/cork joints

For these joints, another step had to be added to the process. The cutting procedure was similar to the one described on Section 3.4.1. However, this time, a thin layer of bio-adhesive was spread on each wood substrate to bond the cork agglomerate sheet on top. After the same curing cycle (8 hours at 50 °C), using weights to apply pressure, the cork-coated surfaces were bonded in the similar way described in Section 3.4.1.

### 3.4.4 Considerations

Ideally, bonding of the joints should be carried out in a dedicated mould, designed for the effect as described by Banea et al. [42] to allow the utilization of a hot-press and ensure that pressure is evenly distributed across the full overlap area. In the first attempts to manufacture the joints such a mould was used, as shown in Figure 26. However, due to the lack of consistency in the thickness of the specimens associated with the use of wood, it was not possible to obtain a flat surface across all the specimens in a single mould. For this reason, pressure could not be evenly distributed across all the joints in the mould and the result was a set of joints where the zero thickness condition was not verified for many of the joints. Alternatively, the utilisation of manual clamps to apply pressure provided similar results to the ones which were obtained from the successfully bonded joints taken from the mould, so, from then on, this method was applied throughout this work.

Figure 26: Mould used for the fabrication of single lap joints.

## 3.5 Additional cork modi cation

To maximise the mechanical performance of the cork layers used in WC joints, a new approach was also explored in this work. Instead of using pre-agglomerated cork sheets for the manufacture of the joints, cork granulates were agglomerated with a bio-adhesive (described in Section 3.1.2) and reinforced with relatively short and randomly dispersed natural ax bres.

The manufacturing process consisted of an alternate manual layup of the materials on top of a 300×300 mm aluminium plate (Figure 27). Thickness control of 1 mm was ensured through the use of silicone sheet. After completing the layup process, a similar plate was placed on top, following a curing procedure in the hot-press for 8 hours, at 50, while applying 0.5 MPa of pressure.

Figure 27: Manufacturing of a reinforced cork layer.

## 3.6 Testing methods

### 3.6.1 Bio-adhesive characterisation

The mechanical and fracture characterisation of an adhesive is crucial to better understand its behaviour and gather the data needed to formulate a cohesive law for a numerical model.

To determine sti ness and strength properties, both the bulk tensile test and thick adherend shear tests (TAST) are generally performed to determine the tensile and shear properties, respectively. Regarding fracture characterisation, double cantilever beam (DCB) and end notched  exure (ENF) tests are performed to obtain fracture toughness in mode I and mode II, respectively.

In the  rst attempts to manufacture a bio-adhesive plate to later obtain bulk specimens, it was soon noted that the adhesive did not e ectively cure with a controlled thickness and in fact left exhibited a large amount of voids. Concurrently, every time a zero thickness condition would not be veri ed in a joint, the substrates would not be properly bonded. Furthermore, the adhesive did not bond to either steel nor aluminium substrates. This limited the characterisation of the adhesive in several ways.

Since true bulk specimens could not be produced with this adhesive, several attempts to obtain the tensile strength via the utilization of modi ed Arcan joints (using thin wood tabs bonded to the steel with an epoxy adhesive as a substrate) in mode I were carried out. However, this also not successful since the Arcan specimen requires a near perfect alignment which cannot be accommodated well by a zero-thickness adhesive layer, resulting in multiple areas devoid of an adhesive bond. Furthermore, delamination occurred in the pine wood whenever a joint was properly bonded ampli ed the di culty of the characterisation.

Despite all of the stated issues, fracture toughness values were able to be determined by modi cation of the traditional test procedures, although through the utilisation of pine wood substrates. Regarding strength, only a single e ective TAST specimen could be produced from oak wood.

### 3.6.2 Thick Adherend Shear Test (TAST)

TAST specimens are speci ed in the international standard ISO 11003-2:2019 and are produced as an adhesive joint with thick hard steel adherends that, when loaded, reduce the amount of peel stresses present, guaranteeing that shear is almost exclusively the only stress state present [42]. Specimen dimensions are speci ed in Figure 28.

Figure 28: Speci cation of a TAST specimen - dimensions in mm [42].

For this work, the relevant standard had to be adapted to t the requirements of the bio-adhesive. Some dimensions were changed due to the zero-thickness condition and the adherends used were machined out of oak wood, instead of the available steel ones. The reason behind the utilisation of oak instead of pine lies in the fact that it is a much harder (and stronger) wood and, therefore, decreases the probability of delamination. This test was carried out in a universal test machine, more speci cally the INSTRON 3367 whose load cell is capable of measuring up to 30 kN. While in the standard procedure digital image correlation (DIC) is commonly used to obtain the strain of the adhesive, the same was not possible in this scenario due to the lack of thickness of the adhesive layer.

### 3.6.3 Single lap joints

The single lap joints manufactured for this work were tested by application of a tensile load on the substrates and were conducted in three di erent test machines, according to the cross-head rate de ned - Quasi-static (Q-S), high cross-head rate (HCR) and impact. The testing campaign is de ned in Table 3. It is crucial to note that, cross-head rate was considered as the key testing parameter in these testing procedures due to the impossibility of calculating the shear strain rate in the adhesive layer, since the zero layer thickness of the layer precludes this calculation.

Table 3: Testing campaign, highlighting the overlap length (imm) tested for each condition.

| | Q-S (0.001 m/min) | HCR (6 m/min) | Impact (60 m/min) |
|---|---|---|---|
| W | 25<br>50 | 50 | 50 |
| DW | 25<br>50 | 50 | 50 |
| WC | 25<br>50 | 50 | 50 |

For the quasi-static tests, the INSTRON® 3367 universal test machine was used and both load and displacement were recorded at a frequency of $10\,s^{-1}$.

Regarding high rate, the tests were carried in the servohydraulic test machine INSTRON® 8801 and, just like before, both load and displacement were recorded but at a frequency of $2000\,s^{-1}$.

As for the impact tests, a dropweight machine was used. A mass of 50 kg was dropped from a height of 51 mm to achieve the desired velocity. The acquisition system recorded load and time at a frequency of $50\,000\,s^{-1}$, although, to measure displacement, digital image correlation (DIC) was required. Thus, part of the bottom clamp was speckled with black and white paint and its movement tracked with a high speed camera, recording at 10 000 frames per second.

### 3.6.4 Mode I and mode II fracture tests

#### Double cantilever beam (DCB) test

In order to determine the fracture energy in mode I, DCB tests were performed with wood substrates and zero-thickness in the bio-adhesive layer. This specimen contains two bonded rectangular beams with equal dimensions. A scheme of the specimens relevant dimensions and loading conditions can be observed in Figure 29. In Figure 30 a image of an actual specimen is presented.

Figure 29: Schematic representation of a DCB test.

Moreover, it is worth mentioning that in this type of test several dimensional parameters can be changed such as:

$a_0$, the length from the loading pins to the end of the region without adhesive, referred to as pre-crack length;

h, the thickness of each adherend;

t the adhesive thickness.

Figure 30: DCB specimen produced.

Regarding the data acquisition, both the load and displacement were recorded. Then, critical energy release rate in mode I, $G_{Ic}$, can be determined by means of an adequate data reduction scheme, presented in the Subsection 3.7.

End notched  exure (ENF) test

To obtain fracture energy in mode II, ENF tests were performed using the same specimens as previously described for the DCB test. However, these specimens are loaded under a di erent con guration, as seen in Figure 31.

Figure 31: Schematic representation of a ENF test, dimensions in millimetres.

Similarly to the previously described test method, there are several key dimensional parameters:

$a_0$, is the initial crack length;

$P$, the load applied;

, the displacement recorded at the centre of the ENF specimen;

$h$, the height of each substrate;

$L$, the horizontal distance from each support to the load application point;

$t$, the adhesive thickness.

Once again, both the load and displacement were recorded and, afterwards, the critical energy release rate in mode II, $G_{IIc}$, is determined with an appropriate data reduction scheme, presented in the Subsection 3.7.

Figure 32: ENF specimen testing setup.

## 3.7 Data reduction scheme

To obtain the energy release rate in mode I and mode II a data reduction scheme must be implemented [43]. There are two classical methods, the Compliance Calibration Method (CCM) [44, 45], based on the Irwin-Kies equation:

$$G_I = \frac{P^2}{2b}\frac{dC}{da} \tag{6}$$

where cubic polynomials are used to t the compliance ($C = C_3 \quad a^3 + C_2 \quad a^2 + C_1 \quad a + C_0$) as a function of the crack length (a), and the Corrected Beam Theory (CBT) [45 49], also derived from the previous equation:

$$G_I = \frac{3P}{2b(a + j \quad j)} \tag{7}$$

but with a correction factor , proposed in 1992 by Wang and Williams [46], to take into consideration the crack tip rotation and de ection:

$$= h\sqrt{\frac{1}{13k}\frac{E_x}{G_{xy}} \quad 3 \quad 2 \quad \frac{}{1 + }^{2}} \quad ; \text{ with } \quad = \frac{p\overline{E_x E_y}}{kG_{xy}} \tag{8}$$

where h is the thickness of the substrate, $E_x$ and $G_{xy}$ its longitudinal normal and shear modulus, $E_y$ the modulus in the thickness direction, and k the shear stress distribution constant for correcting the de ection originated by the shear forces.

To determine the crack length correction a linear regression can be obtained experimentally after loading the specimens at three di erent load levels, graphically represented in Figure 33.

Figure 33: Graphic representation of the method used to determine the crack length correction, . Adapted from [11].

Nevertheless, both these methods require the assessment of the exact crack

length, increasing the di culty of their implementation, especially when a sudden crack propagation occurs and/or when analysing mode II fracture [10, 44, 45].

Bearing in mind that, in reality, the crack tip does not fully behave according to linear elastic fracture mechanics processes, the consideration of a fracture process zone (FPZ) is needed. This FPZ is observed in Figure 34, and develops ahead of the major crack tip caused by plasticisation and nucleation of several micro-cracks. The severity of the phenomenon increases with the ductility of the material since the energy dissipated in the FPZ increases making so that the it must be taken into account in the data reduction scheme [43].

Taking these facts into account, the use of the compliance-based beam method (CBBM) is the preferred process to treat the fracture toughness data, due to the fact it is based on the concept of equivalent crack length, which takes into consideration the phenomena previously described [43, 50], and only depends on the compliance of the specimen during the duration of the test.

Figure 34: Schematic representation of the equivalent crack length and fracture process zone concepts. Adapted from [43].

Using this method, the energy release rate in mode I is de ned as [43]:

$$G_I = \frac{6P^2}{b^2h}\left(\frac{2a_{eq}^2}{h^2E_f} + \frac{1}{5G_{13}}\right) \tag{9}$$

being $P$ the applied or measured load depending on the type of loading condition, $b$ is the width of each specimen, $h$ is the specimen height, $G_{13}$ is the respective shear modulus of the substrates, $a_{eq}$ is the equivalent crack length, whose value is given by the solution of an equation derived from Timoshenko's beam theory [43]:

$$C = \frac{}{P} = \frac{8a_{eq}^3}{bh^3E_f} + \frac{12a_{eq}}{5G_{13}bh} \tag{10}$$

and $E_f$ is the corrected exural modulus, the purpose of which is to correct the fact that this method does not take into consideration the stress concentration and

substrates' rotation close to the crack tip [43]:

$$E_f = C_0 \quad \frac{12(a_0 + j \quad j)}{5bhG_{13}} \quad {}^{1} \; \frac{8(a_0 + j \quad j)^3}{bh^3} \tag{11}$$

being 0 the index set for initial values - where $a_0$ is the initial crack length previously de ned for each method in subsection 3.6 and $C_0$ the initial linear compliance - and a correction factor for the crack length derived from the one used in the CBT method given by the Equations 8, considering an isotropic material and 0.85 for the constant k [51].

Mode II fracture energy can be determined by [52]:

$$G_{II} = \frac{9P^2 a_{eq}^2}{16b^2 E h^3} \tag{12}$$

where

$$a_{eq} = \frac{a_0^3 C_c}{C_{0c}} + \frac{C_c}{C_{0c}} \quad 1 \quad \frac{2L^3}{3} \quad {}^{1=3} \tag{13}$$

with

$$C_c = C \quad \frac{3L}{10bhG_{13}} \tag{14}$$

and

$$E = \frac{3a_0^3 + 2L^3}{8bh^3 C_{0c}} \tag{15}$$

being L half of the ENF specimen total length and index c indicates the corrected value of a variable.

# 4 Numerical details

## 4.1 General considerations

Aiming to successfully predict the behaviour of the single lap joints tested experimentally, a static numerical model was developed for single lap joints with natural pine wood adherends. The adhesive layer was modelled with cohesive elements. These elements' behaviour was dictated by a triangular cohesive law that was de ned via strength and fracture properties partially determined experimentally. Wood substrates were modelled as orthotropic with elastic properties obtained from Table 1. Nevertheless, a layer of cohesive elements was placed within 0.2 mm of the interface to allow potential delamination to occur. These elements were governed by a triangular cohesive law, de ned by strength and fracture properties of natural pine wood determined experimentally by Moura and Dourado [13]. A scheme of the model is presented in Figure 35.

Figure 35: Illustration of the numerical model.

Regarding the de nition of a triangular cohesive law to model damage in timber, experimental results from Moura et al. [13] were used and included not only elastic and strength properties (Tables 1 and 2) but also required fracture properties such as $G_{Ic}$ and $G_{IIc}$. For the modelling of the bio-adhesive's cohesive law $G_{Ic}$ and $G_{IIc}$ values were obtained experimentally in this work. Elastic and strength properties were only estimated, based on the on the brittle behaviour of the adhesive and considering a minimum strength in mode II of 12.40 MPa as seen in Section 5.1.1.

## 4.2 Boundary conditions

The boundary conditions were set by de ning one of the edges as pinned and by applying a displacement to the opposite edge, reproducing the actual testing conditions. These conditions are shown in Figure 24.

Figure 36: Illustration of the boundary conditions applied.

## 4.3 Mesh

The mesh utilised for the simulation was highly re ned and the elements were distributed with a bias towards the areas where stresses concentration are higher, as observed in Figure 25. CPS4R plane stress elements were used for the elastic area of wood and COH2D4 cohesive elements were used for the cohesive layers.

Figure 37: Mesh used in the simulations.

# 5 Results and discussion

In this chapter, results from work that are not included in the appended paper are presented and discussed.

## 5.1 Bio-adhesive characterisation

As aforementioned, the only tests which allowed for the successful characterisation of the bioadhesive were the TAST and the DCB. The main results of these tests are presented below.

### 5.1.1 TAST

As stated in Section 3.6.2, the impossibility of using the bioadhesive in conjunction with metallic substrates, allied to the frequent delamination of pine timber, led to the use of oak as the adherend material for a TAST test. The oak samples were manually machined to the dimensions of the conventional substrates (Figure 38).

(a) TAST specimen.

(b) TAST setup.

(c) TAST specimen after failure.

Figure 38: TAST specimen before and after the test performed.

The results of the test are presented on Figure 39.

Figure 39: Shear stress - displacement curve of the TAST specimen tested.

As referred in Section 3.6.2, the strain on the adhesive layer could not be measured due to the lack of thickness of the adhesive layer. Nevertheless, the results show a maximum stress of 12.40 MPa, which can be interpreted as a minimum value for the shear strength of the bio-adhesive, since the joint still failed by delamination.

### 5.1.2 DCB

To obtain the critical energy release rate in mode I, DCB tests were performed as described in Section 3.6.4. Data from the P-curve was processed using CBBM to obtain a R-curve and, therefore $G_{Ic}$. Representative P- and R-curves from one of the tests are presented in Figures 40 and 41. Fracture surfaces are shown in Figure 42. The average value obtained for $G_{Ic}$ was 0.16 0.05 N/mm.